This article has been accepted for inclusion in a future issue of this journal. Content is final as presented, with the exception of pagination.

A New Generalized Multisource Inverter for Electric Vehicles Controlled by Model Predictive

Mohammad Ali Hosseinzadeh, *Member, IEEE*, Maryam Sarebanzadeh, *Member, IEEE*, Cristian F. Garcia, *Senior Member, IEEE*, Ebrahim Babaei, *Senior Member, IEEE*, Jose Rodriguez, *Life Fellow, IEEE*, and Ralph Kennel, *Senior Member, IEEE*

***Abstract*—A multisource inverter comprises multiple dc sources in the input that can be combined with varying voltage levels to operate under different loads and reduce the battery capacity requirements of electric vehicles. This article introduces a generalized topology for multisource inverters (MSIs) aimed at reducing the number of power electronics switches, lowering voltage stress on power switches, and minimizing the battery size. A dual-source inverter, based on the proposed generalized configuration, can generate four combinations that reduce the battery size of electric vehicles (EVs) while minimizing power losses. To harness the advantages of model predictive control, the proposed dual-source traction inverter is controlled using this method. The feasibility of the proposed approach is validated through simulation results, which demonstrate its suitability as a drive for an electric motor. The outcomes indicate that model predictive control is a viable alternative for such applications, offering simplicity, high performance, and low harmonic content. Furthermore, experimental results for a static load are presented to verify the correct operation of the proposed system.**

***Index Terms*—Electric vehicles (EVs), model predictive control, multisource inverters (MSIs).**

I. Introduction

IN THE past few decades, electric vehicles (EVs) have gradually gained acceptance with promising performance [1], [2]. EVs can diminish or exclude dependence on oil by using other energy sources, depending on their degree of electrification [3]. Most commercial vehicles use traditional voltage source inverter (VSI) as traction inverters because of their low cost, high power density, and simple control [4]. The power circuit of a standard two-level VSI is shown in Fig. 1(a). However, VSI indicates some restrictions due to the wide range of electric machine (EM) performance and the need for high power. In fact, VSI produces low performance at low loads, and EM performance is restricted by the fixed battery voltage. As an alternative solution, some original equipment manufacturers use a dc–dc converter to provide variable input voltage to the VSI, as shown in Fig. 1(b) [5]. This can improve the performance of EMs, along with inverter and EM performance. However, this configuration also has drawbacks in terms of price and power density. In addition, the power rating of the dc–dc converter must be identical to the battery pack because they are connected in series. Therefore, increasing the range of electric driving with the increasing power of the battery pack requires more transactions as opposed to the simple design. Several new inverter configurations for high-voltage applications have been reported in the literature, such as multilevel inverters [6], [7]. They offer some advantages, such as low total harmonic distortion (THD) and low power losses, compared with two-level inverters. Among new inverter topologies, the Z-source inverter furthers its reputation for electric propulsion systems since it also offers an adjustable step-up in voltage to the load without the use of a dc–dc converter [8]. Fig. 1(c) depicts the power circuit of a Z-source inverter. However, they negatively affect using larger volumes of passive components or more components than a standard VSI. Therefore, the complexity of their control and cost prevent them from being commercialized in traction drive systems. To overcome conventional and new inverter configurations, one concept called the multisource inverter (MSI) has recently been introduced for the first time in [9]. The aim of introducing this type of inverter for e-mobility applications, such as EVs, is to deliver ac power to EMs similar to that of standard two-level inverters using a single power conversion stage. An MSI comprises several dc sources at the input that can be combined with varying voltage levels to operate under different loads. MSIs offer the ability to connect several different dc sources with varying voltage levels to the output load. Because of its ability to connect a variable dc-link voltage to the load, the multisource reduces switching losses and provides a viable alternative to EV

Manuscript received 19 February 2023; revised 26 May 2023, 2 August 2023, and 30 September 2023; accepted 18 October 2023. This work was supported in part by the ANID/FONDECYT through Regular Research under Grant 1210208 and in part by the Basal under Grant FB0008 (AC3E). *(Corresponding author: Mohammad Ali Hosseinzadeh.)*

Mohammad Ali Hosseinzadeh, Maryam Sarebanzadeh, and Ralph Kennel are with the Chair of High-Power Converter Systems, Technical University of Munich, 80333 Munich, Germany (e-mail: mohammad-ali.hosseinzadeh@tum.de; maryam.sarebanzadeh@tum.de; ralph.kennel@tum.de).

Cristian F. Garcia is with the Faculty of Engineering, Universidad de Talca, Talca , Chile (e-mail: cristian.garcia@utalca.cl).

Ebrahim Babaei is with the Faculty of Electrical and Computer Engineering, University of Tabriz, Tabriz 5166616471, Iran, and also with the Engineering Faculty, Near East University, 99138 Nicosia, Türkiye (e-mail: e-babaei@tabrizu.ac.ir).

Jose Rodriguez is with the Faculty of Engineering, Universidad San Sebastian, Santiago 8420524, Chile (e-mail: j.rodriguez@uss.cl).

Color versions of one or more figures in this article are available at https://doi.org/10.1109/TIE.2023.3329248.

Digital Object Identifier 10.1109/TIE.2023.3329248

This article has been accepted for inclusion in a future issue of this journal. Content is final as presented, with the exception of pagination.

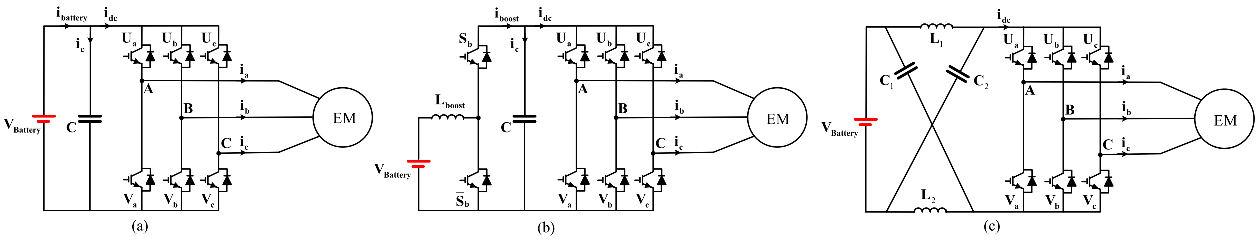

Fig. 1. VSI-base configurations in EVs applications. (a) Standard VSI. (b) dc/dc boost converter integrated with VSI. (c) Z-source converter integrated with VSI.

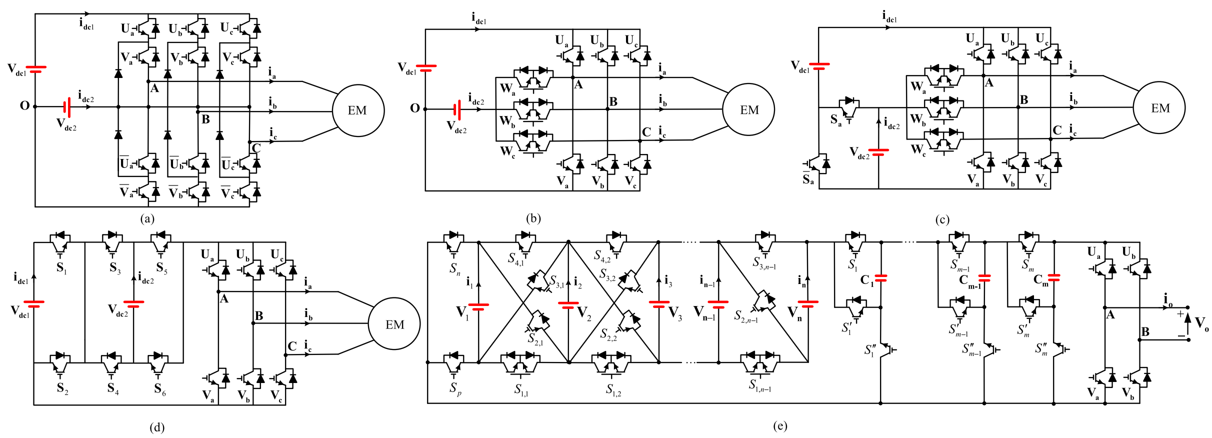

Fig. 2. MSI configurations in EVs applications. (a) Neutral-point clamp (NPC) MSI [9]. (b) T-type MSI [10]. (c) ReMSI multisource configuration [11]. (d) Reconfiguration HES-MSI with two-dc sources [12]. (e) Single-phase switched-capacitor MSI for photovoltaic systems [13].

applications. In [9] and [10], two MSI configurations have been introduced that use two dc sources in the input, as shown in Fig. 2(a) and (b). Depending on the load demand, they supply the load with either a high-voltage battery pack or a low-voltage battery pack, which is in fact a two-level natural diode-clamp inverter or a T-type inverter. Hence, the two dc sources can produce three different operation modes: $V_1, V_2,$ and $V_2 - V_1$. The drawback of these MSIs is that the two dc sources used cannot be connected in series to achieve a higher overall dc-link voltage, which leads to reduced efficiency. Furthermore, in EV applications, they need a battery pack with a high capacity, which causes increased cost and high volume and weight. In addition, the current extracted from the battery pack by high-current loads remains unchanged when compared with the scenario where the battery is solely connected to the load through a rigid dc-link inverter. As depicted in Fig. 2(c), a new MSI topology, known as the reconfigurable multisource inverter (ReMSI), has been developed in [11]. This topology offers the advantage of interconnecting dc input sources in series, allowing the dc-bus voltage to exceed that of any individual source. Namely, it can generate one more operation mode ($V_1, V_2, V_2 - V_1,$ and $V_1 + V_2$) by adding two extra switches. This can further reduce switching losses and allow the traction system to maintain even more torque at engine speed. The ReMSI requires a high number of power switches to operate in four different modes that can be obtained with two used dc sources, which causes high losses, reduces efficiency, and increases weight and volume.

For EV energy storage systems, an MSI topology with a generalized structure was presented in [12]. This topology, similar to [11], when using two dc sources [see Fig. 2(d)], can combine all possible dc-link source combinations, which provide a second mode that increases the dc source input voltages. Therefore, the voltage rating of dc sources may be specifically created, which reduces the need for cell balancing for both sources. Also, when the dc source with a low voltage rating is replaced by a supercapacitor, it reduces the size of the battery pack for EVs by almost 25%. However, this MSI structure [12] faces a high number of operating active switches, which raises conduction losses and diminishes its efficiency. In addition, the voltage stress of the switches is high, which affects the final cost of the inverter. Two multisource switched-capacitor multilevel inverters (MLIs) were presented by Hosseinzadeh et al. [13]. The introduced MLI has been proposed for single-phase photovoltaic applications to boost the low input voltage of photovoltaic (PV) by combining a multisource unit and a switched capacitor unit, as shown in Fig. 2(e). Another benefit of this topology is that it reduces the number of power switches and capacitors compared with other similar MLIs that have a generic topology and use switched capacitors. Although capacitors charge and discharge with series and parallel methods without the need for any sensors, they have a main drawback, which is that they inrush current and cannot be used for high-power applications. In addition, it cannot be applied to EVs due to the use of a switched-capacitor unit.

This article has been accepted for inclusion in a future issue of this journal. Content is final as presented, with the exception of pagination.

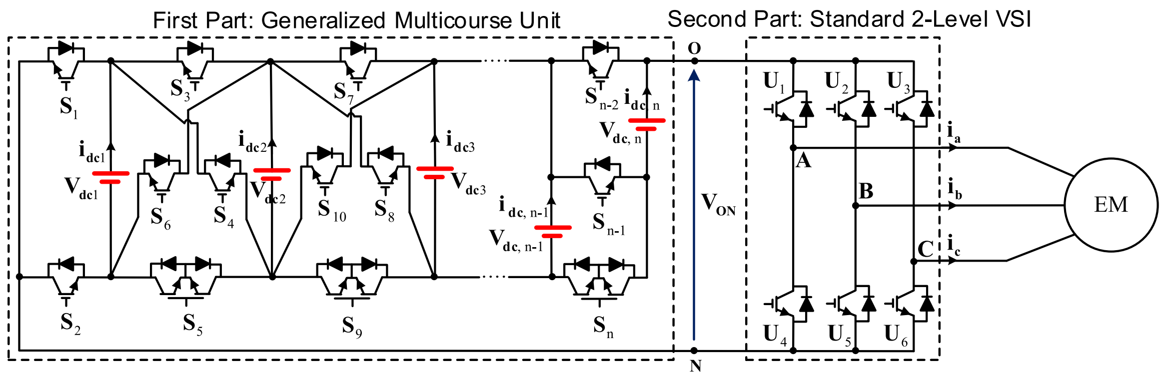

Fig. 3. Proposed generalized MSI topology with n number of dc sources.

This article proposes the use of a generalized topology for an MSI in an EV drive. The main contribution of the article is as follows.

1) Proposing a new generalized MSI topology with fewer conductive active switches in current paths, capable of utilizing all combinations of multisource and handling bidirectional power flow for EV energy storage systems.
2) Proposing an model predictive control (MPC) technique for controlling the proposed multisource inverter in an EV system, which reduces harmonic distortion and minimizes power losses.

The rest of this article is organized as follows. In Section II, the generalized multisource traction inverter topology is introduced with an explanation of all operation modes. Then, the main features of the suggested topology and its mathematical model are explained in Section III. In Section IV, a model-predictive control is applied for control of the system. In Section V, a comparative comparison is made based on various characteristics, power losses, and efficiency between the proposed MSI and other classical MSIs. In Section VI, simulation results for a permanent magnet synchronous machine are provided in order to evaluate the performance of the proposed MSI. Finally, Section VII concludes this article.

II. Proposed MSI Topology

A. Generalized Topology

The proposed generalized MSI topology is displayed in Fig. 3. As you can see, it consists of two parts: a multisource unit and a standard two-level VSI. The multisource units are comprised of several dc voltage sources that, in an EV, can be batteries with different powers. The proposed MSI topology is designed such that it can combine all possible combinations of the dc voltage sources. Therefore, based on the dc voltage source values, the proposed MSI can work in different operation modes. In order to have maximum operation mode, the dc voltage source values are selected in trinary values as follows:

$$V_{\mathrm{dc},1} = V_{\mathrm{dc}} \tag{1}$$

$$V_{\mathrm{dc},2} = 3V_{\mathrm{dc}} \tag{2}$$

$$V_{\mathrm{dc},3} = 9V_{\mathrm{dc}} \tag{3}$$

$$V_{\mathrm{dc},j} = 3^{j-1}V_{\mathrm{dc}} \quad \text{for} \quad j = 1, 2, \ldots, n. \tag{4}$$

Hence, the maximum number of operation modes $N_{\mathrm{op,mode}}$ of the proposed MSI in terms of dc voltage source quantity is given by

$$N_{\mathrm{op,mode}} = \sum_{j=1}^{n} \frac{V_{\mathrm{dc},j}}{V_{\mathrm{dc}}} = \frac{3^n - 1}{2}. \tag{5}$$

The maximum voltage stress (MVS) of the power switch depends on the maximum voltage across the switch. Since the proposed MSI is comprised of two parts, the MVS of each switch at each part is computed separately in the following. The MVS of multisource (MS) unit switches depends on the input dc voltage source magnitudes, which are computed for $j \geq 2$ using the following relations:

$$V_{S_1} = V_{S_2} = V_{\mathrm{dc}1} \tag{6}$$

$$(V_{S_3} = V_{S_6}) = (V_{S_7} = V_{S_{10}}) = \cdots = V_{\mathrm{dc},j} \tag{7}$$

$$(V_{S_4} = V_{S_5}) = (V_{S_8} + V_{S_9}) = \cdots = V_{\mathrm{dc},j-1}. \tag{8}$$

Therefore, the maximum blocking voltage of the MS unit of the topology is calculated using (6)–(8) and is expressed by (9)

$$V_{\mathrm{block,MS}} = [3^n - 2]V_{\mathrm{dc}}. \tag{9}$$

The maximum blocking voltage of the power switch of the second part of the proposed MSI, which is a standard VSI endures the maximum output voltage; therefore, it is expressed as

$$V_{\mathrm{block,VSI}} = 3[3^n - 1]V_{\mathrm{dc}}. \tag{10}$$

Therefore, the total blocking voltage (TBV) of the proposed MSI is the sum of (9) and (10) and can be expressed by (11) as follows:

$$V_{\mathrm{block,MSI}} = [4(3^n) - 5]V_{\mathrm{dc}}. \tag{11}$$

B. Dual-Sources Traction Inverter

The power circuit of a dual-source inverter based on the proposed generalized MSI is shown in Fig. 4. It comprises two dc sources that are utilized for the input of a standard two-level VSI. Five used power switches (S_1–S_5) produce variable dc voltage, which is used as the input dc-link of the VSI. All power switches are unidirectional insulated gate bipolar transistors (IGBTs) with a parallel diode, which can provide the bidirectional operation of

This article has been accepted for inclusion in a future issue of this journal. Content is final as presented, with the exception of pagination.

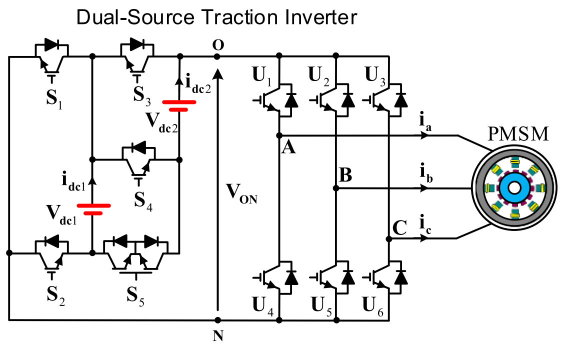

Fig. 4. Power circuit of the proposed dual-source traction inverter.

TABLE I
FOUR OPERATION MODES OF THE PROPOSED MSI BASED ON DC VOLTAGE SOURCES

Modes	S_1	S_2	S_3	S_4	S_5	V_{ON}
I	OFF	ON	ON	OFF	OFF	V_{dc1}
II	ON	OFF	OFF	OFF	ON	$V_{dc2} - V_{dc1}$
III	OFF	ON	OFF	OFF	ON	V_{dc2}
	ON	OFF	OFF	ON	OFF	
IV	OFF	ON	OFF	ON	OFF	$V_{dc1}+V_{dc2}$

the inverter, except for S_5 which is a bidirectional power switch consisting of two IGBTs with two parallel diodes. The maximum combination of two dc sources to produce a positive voltage is four combinations, so the proposed MSI can create the maximum combinations only with five power switches. According to the firing of the five power switches, four distinct operation modes can be defined for the proposed MSI. All operation modes are given in Table I and Fig. 5 based on the possible switching states, and they are also illustrated in detail in the following.

1) *First Operation Mode:* In this mode, by turning ON two power switches (S_2 and S_3) the only V_{dc1} is used as a dc-link voltage of VSI, as shown in Fig. 5(b). Therefore, V_{dc1} supplies the power to transfer the load, and no power is extracted from V_{dc2}. In this mode, the magnitudes of V_{dc1} are preserved, so it is utilized for light loads that require less power.
2) *Second Operation Mode:* By turning ON two power switches (S_1 and S_5) both dc sources provide power to the load. Hence, both dc sources are connected in series, and the voltage utilized in the load is $V_{dc2} - V_{dc1}$, as shown in Fig. 5(c).
3) *Third Operation Mode:* In this mode, only V_{dc2} is used as a dc-link voltage of VSI by turning ON two power switches (S_2 and S_5). Therefore, V_{dc2} supplies the power to transfer the load, so V_{dc1} is not applied, as shown in Fig. 5(d) and (e).
4) *Fourth Operation Mode:* By turning ON two power switches (S_2 and S_4), both dc sources provide power to the load concurrently. As a result, both dc sources are linked in series, and the voltage in the load is $V_{dc1} + V_{dc2}$.

In the proposed MSI topology, the two independent dc sources can be connected to different capacitor banks. Fig. 6 illustrates the torque–speed characteristic of an electric motor when the proposed MSI is employed. As it indicates, in low-speed and low-torque operation, the first mode can be achieved by transferring the power to the motor with a single dc source V_{dc1}. The second operating mode is produced by speeding up the motor and increasing the torque. For high speed and high torque, the maximum dc-link voltage, which is $V_{dc1} + V_{dc2}$ transfers the power to the motor.

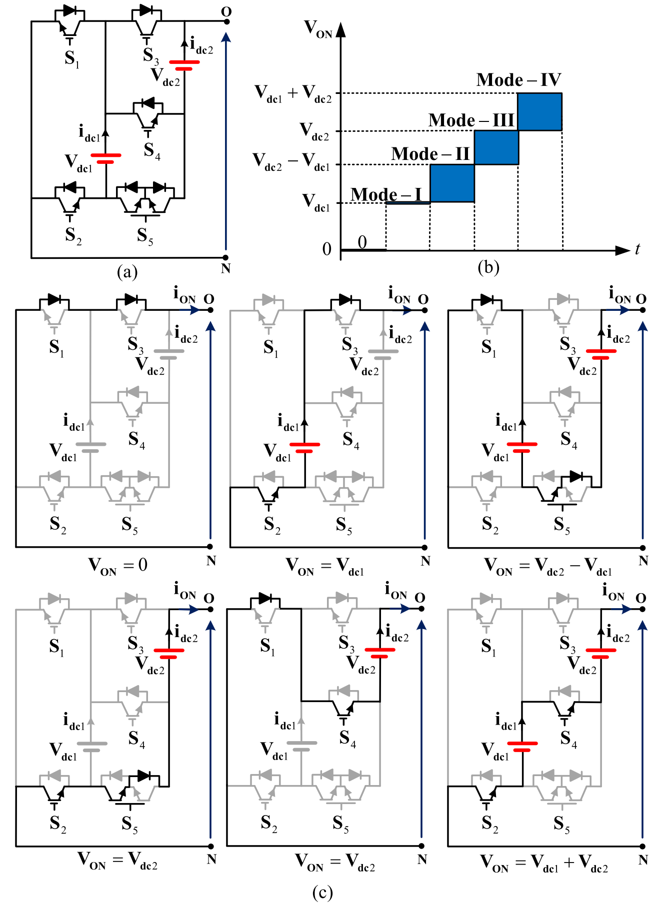

Fig. 5. (a) First part of proposed MSI. (b) Output voltage of V_{ON}. (c) Produced four operation modes by the proposed first part of the proposed MSI.

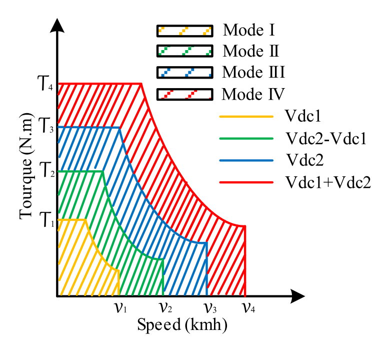

Fig. 6. Speed–torque characteristic of electrical motor.

The MVS of each power switch for the first part of the proposed MSI can be obtained from (6)–(8) as

$$V_{S_1} = V_{S2} = V_{S4} = V_{S5} = V_{dc1} \tag{12}$$

$$V_{S_3} = V_{\text{dc}2}. \quad (13)$$

The voltage stress of all power switches for the second part of MSI is a standard VSI equal to $(V_{\text{dc}1} + V_{\text{dc}2})$. Therefore, the TBV of the proposed MSI with two dc sources is

$$\text{TBV} = 10V_{\text{dc}1} + 7V_{\text{dc}2}. \quad (14)$$

III. Mathematical Model of Proposed MSI

In order to explain in a simple way how to calculate the mathematical model of the proposed MSI, we divided it into two parts. The first part is a multisource structure that combines two dc power sources to provide five positive voltage levels (plus a zero voltage level), while the second part is a typical VSI. By examining the equivalent circuits for the switching states and formulating an equation for each output voltage component in terms of the gating signals, it is possible to establish a general expression for the output voltage of the first half of the proposed MSI. The variable voltage, V_{ON}, is defined as the output voltage produced by the first part of the proposed MSI, and that can be determined as a function of the switches' gate signals and the two dc voltages

$$V_{\text{ON}} = XV_{\text{dc}1} + YV_{\text{dc}2}. \quad (15)$$

The function of X and Y are related to the state of power switches can be expressed

$$X = (U_{S_2} \oplus U_{S_5})(U_{S_2} - U_{S_5}) \quad (16)$$

$$Y = (U_{S_4} \vee U_{S_5}). \quad (17)$$

Here, $U_{S_2}, U_{S_4},$ and U_{S_5} are the switching functions of power switches of $S_2, S_4,$ and S_5, it means U_{S_j} is "ON" if S_j is ON and U_{S_j} is "OFF" if S_j is OFF ($j = 2, 4, 5$). In (16) and (17) "$\oplus$" is XOR sign and "$\vee$" is OR sign in Boolean logic.

The second part's mathematical model, a typical VSI, can be written as follows:

$$V_{AN} = V_{\text{ON}}\mathbf{U_a}$$

$$V_{BN} = V_{\text{ON}}\mathbf{U_b}$$

$$V_{CN} = V_{\text{ON}}\mathbf{U_c}. \quad (18)$$

With the following definition of the switching function of power switches in VSI:

$$\mathbf{U_a} = \begin{cases} 1 & \text{if } U_1 \text{ is } on \text{ and } U_4\ off \\ 0 & \text{if } U_1 \text{ is } off \text{ and } U_4\ on \end{cases} \quad (19)$$

$$\mathbf{U_b} = \begin{cases} 1 & \text{if } U_2 \text{ is } on \text{ and } U_5\ off \\ 0 & \text{if } U_2 \text{ is } off \text{ and } U_5\ on \end{cases} \quad (20)$$

$$\mathbf{U_c} = \begin{cases} 1 & \text{if } U_3 \text{ is } on \text{ and } U_6\ off \\ 0 & \text{if } U_3 \text{ is } off \text{ and } U_6\ on. \end{cases} \quad (21)$$

The three-phase line-to-ground voltage $[V_{An}, V_{Bn}, V_{Cn}]$ is calculated as follows:

$$\begin{bmatrix} V_{An} \\ V_{Bn} \\ V_{Cn} \end{bmatrix} = \frac{1}{3}\begin{bmatrix} 2 & -1 & -1 \\ -1 & 2 & -1 \\ -1 & -1 & 2 \end{bmatrix} \times \begin{bmatrix} V_{AN} \\ V_{BN} \\ V_{CN} \end{bmatrix}. \quad (22)$$

TABLE II
Inverter Line Voltage for Each Switching State and dq-Frame

V_{ON}	$\mathbf{U_a}$	$\mathbf{U_b}$	$\mathbf{U_c}$	V_{AB}	V_{BC}	V_{CA}	dq-frame
MS Output Voltage	OFF	OFF	OFF	0	0	0	[0 0 0]*M
	ON	OFF	OFF	V_{ON}	0	-V_{ON}	[1 0 -1]*M
	ON	ON	OFF	0	V_{ON}	-V_{ON}	[0 1 -1]*M
	OFF	ON	OFF	V_{ON}	V_{ON}	0	[1 1 0]*M
	OFF	ON	ON	-V_{ON}	0	V_{ON}	[-1 0 1]*M
	OFF	OFF	ON	0	-V_{ON}	V_{ON}	[0 -1 1]*M
	ON	OFF	ON	V_{ON}	-V_{ON}	0	[1 -1 0]*M
	ON	ON	ON	0	0	0	[1 1 1]*M

Therefore, the line-to-line voltages $[V_{AB}, V_{BC}, V_{CA}]$ are calculated through well-known formulas

$$V_{AB} = V_{An} - V_{Bn}$$

$$V_{BC} = V_{Bn} - V_{Cn}$$

$$V_{CA} = V_{Cn} - V_{An}. \quad (23)$$

Table II illustrates the device switching states and the input dc voltage applied to the load regarding the different operating modes. To create mode II, the magnitude of the output of MSI is equal to $V_{\text{dc}2} - V_{\text{dc}1}$, and the voltage $V_{\text{dc}2} > 2V_{\text{dc}1}$ is selected.

IV. MPC for the Proposed MSI

A. Permanent Magnet Synchronous Motor Model

The dynamic space state model of the permanent magnet syncronous machine (PMSM) in a synchronous dq-frame oriented with the rotor position angle θ_r is the following [14]:

$$\dot{\mathbf{x}} = A(x) + B(u) \quad (24)$$

$$A = \begin{bmatrix} -\frac{R_s}{L_s} & \omega_r & 0 & 0 \\ -\omega_r & -\frac{R_s}{L_s} & -\frac{\psi_m}{L_s} & 0 \\ 0 & \frac{3}{2J_m}\psi_m p^2 & -\frac{B_m}{J_m} & 0 \\ 0 & 0 & 1 & 0 \end{bmatrix}, B = \begin{bmatrix} \frac{1}{L_s} & 0 \\ 0 & \frac{1}{L_s} \\ 0 & 0 \\ 0 & 0 \end{bmatrix} \quad (25)$$

$$\dot{\mathbf{x}} = \begin{bmatrix} \dot{i}_d \\ \dot{i}_q \\ \dot{\omega}_r \\ \dot{\theta}_r \end{bmatrix}, x = \begin{bmatrix} i_d \\ 1_q \\ \omega_r \\ \theta_r \end{bmatrix}, u = \begin{bmatrix} v_d \\ v_q \end{bmatrix}. \quad (26)$$

The parameters of the PMSM are R_s stator resistor, L_s stator inductance, ψ_m the magnitude of the flux generated by the rotor magnet, p number of poles, J_m inertia, and B_m the friction of the machine.

The voltages of the dq-frame v_d and v_q are obtained from the transformation of (15), which is the output voltage of MSI in the abc-frame [15].

The electric torque of PMSM is obtained as follows:

$$T_e = \frac{3}{2}p\psi_m i_q. \quad (27)$$

The relation between the electric and load torque of the machine is given by

$$T_e - T_L = J_m\frac{d\omega_m}{dt} - B_m\omega_m \quad (28)$$

This article has been accepted for inclusion in a future issue of this journal. Content is final as presented, with the exception of pagination.

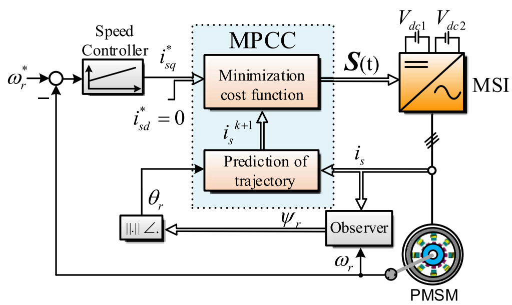

Fig. 7. MPC control scheme for the proposed MSI.

TABLE III
COMPARISON OF THE PROPOSED MSI WITH VSI AND OTHER MSIS

Specifications	VSI	[9]	[10]	[11]	[12]	[P]
No. of operational modes	1	3	3	4	4	**4**
No. of input DC sources	1	2	2	2	2	**2**
No. of bidirectional switches	0	0	3	5	0	**1**
No. of unidirectional switches	6	12	6	6	12	**10**
No.of total IGBTs	6	12	12	16	12	**12**
No.of total diodes	6	18	12	16	12	**12**
No.of gate drivers	6	12	9	11	12	**11**
Maximum no. of active switches	2	4	3	4	5	**4**
TBV× V_{dc}	6	48	30	34	34	**31**
Generalized	No	No	No	No	Yes	**Yes**

where ω_m is the mechanical speed, and T_L is the load torque.

B. Model Predictive Control for the Proposed MSI

The overall scheme of the proposed MPC is shown in Fig. 7. By using a rotating dq-reference frame oriented to the rotor magnetic field axis, each stator current component has a physical meaning. The imaginary component i_q is proportional to the electric torque while the real component i_d is proportional to the reactive power. In this way, the machine control is implemented as a current control scheme, where the current references are generated by the external speed control loop [16]. The model of the machine is used for predicting the behavior of the stator currents, and the cost function must consider the error between the reference currents and predicted currents. By using the Euler approximation for the stator current derivatives [17] for a sampling time T_s, that is

$$\frac{di}{dt} \simeq \frac{i(k+1)-i(k)}{T_s}. \tag{29}$$

The predicted stator currents in the dq-reference frame are obtained from (24)–(26) as follows:

$$i_q^p(k+1) = \left(1-\frac{R_sT_s}{L_s}\right) i_q(k) + T_s\omega_r i_d(k) - \frac{\psi_m\omega_rT_s}{L_s} + \frac{T_s}{L_s}v_q(k) \tag{30}$$

$$i_d^p(k+1) = \left(1-\frac{R_sT_s}{L_s}\right) i_d(k) + T_s\omega_r i_q(k) + \frac{T_s}{L_s}v_d(k). \tag{31}$$

In Fig. 7, a proportional integral (PI) controller is used for speed control and generates the reference for the torque-producing current, i_q^*. A predictive current controller is used to track this current. In the predictive scheme, the discrete-time model of the machine is used for predicting the stator current components for the seven different voltage vectors generated by the inverter. The voltage vector that minimizes a cost function is selected and applied during a whole sampling interval. The objectives of the predictive current control scheme are torque current reference tracking, torque by ampere optimization, and current magnitude limitation. These objectives can be expressed as the following cost function:

$$g = (i_d^p(k+1))^2 + (i_q^* - i_q^p(k+1))^2. \tag{32}$$

V. COMPARISON STUDY

A. Comparison Components and Operation Modes

A comparison study is carried out in different aspects between the proposed [P] MSI, standard VSI, and other recent MSI topologies to show the benefits and limitations. The compared topologies use two dc sources, such as T-type MSIs and neutral-point clamp (NPC)-MSIs [11], [12]. We tried to consider different parameters that have an effect on the performance of the MSIs, such as cost, size, and complexity. The results are given in Table III. This table gives that a standard VSI uses a dc-link (battery) that only has one operating mode. The presented topologies [9] and [10] use two dc sources with up to three operating modes. This means that they can only produce the operating modes $V_{\rm dc1}$, $V_{\rm dc2}$, and $V_{\rm dc2} - V_{\rm dc1}$ and cannot combine these two dc sources in series to achieve a higher overall dc-link voltage. The proposed MSIs [11] and [12] can create another mode that uses the overall dc-link voltage ($V_{\rm dc1} + V_{\rm dc2}$). This allows the dc-bus voltage to be larger than any other source. This enables the traction system to maintain maximum torque at even higher engine speeds while reducing switching losses even further.

As given in Table III, the benefit of the proposed MSI is its extendability, similar to [12] (using n dc sources), in contrast to other topologies [9], [10], [11] that do not have this specification aspect, so this feature is very useful when it is used for energy storage systems in EV applications that extend battery life. Typical EV energy storage systems use the entire battery voltage level to provide power at light or medium loads. In systems that use two dc sources (MSI topologies), the higher magnitude dc source can be a battery, and the lower magnitude dc source can be a supercapacitor [9], [10], [11], [12], which leads to a reduction in the size of the battery pack. In addition, the battery life is increased because it is not using the full power of the battery when the electric motor demands less power. Furthermore, by using n number of dc sources in the proposed MSI and [12], EV battery life is significantly increased. This is due to the fact that depending on the speed of the EV, some of the battery cells transfer the power required by the motor, and other cells are in standby mode [18]. To provide a high number of dc sources in the proposed MSI, for low-value dc sources, a small number of battery cells can be connected in series, and for high-value dc sources, a large number of cells can be connected in series [18], [19]. The limitation of using multisource configurations, such as

This article has been accepted for inclusion in a future issue of this journal. Content is final as presented, with the exception of pagination.

the proposal and [12], is asymmetric operation due to using different sources with different magnitudes. In most configurations in the industry, symmetric operation is used, which makes it easy to control and balance the voltages. But with the development and advancement of control methods, the asymmetric operation can be solved in the future [19], [20]. According to Table III, the proposed MSI has a low number of IGBTs and drivers in comparison to [11] and [12], which generate the same number of operation modes. The low number of switches necessitates ten unidirectional switches in the proposal, resulting in smaller size and cost as well as reduced complexity. In addition, the proposed MSI has a lower number of conductive active switches (4) in the current path compared with [12] (5). Therefore, the low conductivity of the devices leads to low conduction losses, which increase efficiency. Although [11] has the same number of active switches as the proposal, it uses a high number of bidirectional power switches and cannot be extended to a generalized topology to increase battery life. Another advantage of the proposal is the low TBV compared with similar MSI topologies with the same operation modes [11], [12]. Low voltage stress means low manufacturing costs, which is an important factor for the industry's massive production. The TBV for all presented MSIs and the proposal is calculated and given in Table III. Depending on the dc voltage source magnitude in each topology, each switch has a different blocking voltage. Therefore, the blocking voltage of the inverters is calculated per unit (V_{dc}). According to (11), the TBV of the proposal, considering $V_{\text{dc1}} = V_{\text{dc}}$ and $V_{\text{dc2}} = 3V_{\text{dc}}$, is obtained as $31V_{\text{dc}}$. In Table III, the standard VSI achieves a low TBV because of a smaller number of switches (6), in contrast to other MSIs. On the other hand, Dorn-Gomba et al.[9] exhibited a notably high TBV, while [11] and [12] share similar TBV values. The MSI introduced in [10] possesses a minimum TBV of $30V_{\text{dc}}$, whereas the proposed MSI closely aligns with this value at $31V_{\text{dc}}$. Although [10] does have an edge over the proposed MSI in this regard, the proposal boasts a greater number of operation modes, resulting in a more compact battery pack size. The disadvantage of the proposal to reduce blocking voltage is that the switches have different voltage ratings. But this is not an acute problem; for example, in practical applications, the manufacturer chooses the power switches that endure the MVS (in the proposal, they are VSI switches) because other switches have lower voltage stress.

B. Comparison Power Losses and Efficiency

One advantage of the proposal over [12], which has the same operation modes, is the number of ON-state switches in the current path to generate each mode. This feature affects the power losses and the efficiency of the proposed MSI. Table IV gives the conducting switches and parallel diodes of the MS units in the proposed MSI and [12].

As can be seen from this table, the number of ON-state switches and diodes in the proposed MSI is two switches for all operation modes except for the second mode, which is three, so it has fewer conduction devices than [12], which has three devices always in ON-state for each operation mode. Therefore, it results in a reduction in conduction losses, and it is expected

TABLE IV
CONDUCTING ACTIVE SWITCH/DIODE FOR THE PROPOSAL AND [12]

Operation modes	Current direction	Active Switch/Diode of MS unit [12]	Proposed
Mode I	+	S_4, D_5, D_2	S_2, D_3
	-	S_2, D_4, D_5	S_3, D_2
Mode II	+	S_1, D_3, D_6	S_5, D_5, D_1
	-	S_3, S_6, D_1	S_1, S_5, D_5
Mode II	+	S_1, D_3, D_5	S_4, D_1
	-	S_3, D_1, D_5	S_1, D_4
Mode IV	+	S_1, S_4, S_5	S_4, S_2
	-	D_1, D_4, D_5	S_5, D_4

TABLE V
SIMULATION PARAMETERS FOR POWER LOSSES ANALYSIS

Parameters	Values
DC-link voltage	$V_{\text{dc1}} = 150\,[\text{V}]$ $V_{\text{dc2}} = 450\,[\text{V}]$
IGBT (IHW20N120R3FKSA1)	1200 [V], 60 [A]
Load frequency (f_o)	50 [Hz]
Resistive load (R)	10 [Ω]
Inductive load (L)	10[mH]
Sample time (T_s)	40 [μs]

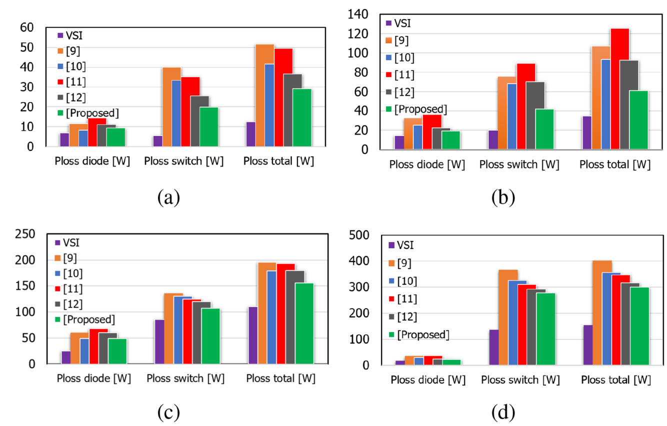

Fig. 8. Power losses evaluations of VSI, the proposed MSI, and other MSIs. (a) First operation mode. (b) Second operation mode. (c) Third operation mode. (d) Fourth operation mode.

that the proposed MSI will have lower conduction losses than [12]. The conduction losses of the second part, which is standard VSI for both topologies, are the same. In order to confirm this future, the power loss and efficiency of the proposed topology are compared with [10], [11], and [12], which use the same number of operation modes. All topologies are simulated in PLECS. We implemented the MPC technique for all three topologies. Table V gives the simulation parameters to investigate the power losses. In this simulation, an IGBT with a voltage rating of 1200 V and a current rating of 60 A (IHW20N120R3FKSA1) is used. The value of the turn-ON resistance of the switches and diodes is considered based on the switch and diode datasheets, which are used for the power loss analysis of the proposed topology, the current–voltage curve of the switch, and the diode for two temperatures of 25°C and 125°C is defined in the software.

The magnitude of dc-link voltages is selected at 1:3. The power losses and efficiency are evaluated for all operation modes. The different operation modes are obtained by changing the amplitude of the reference current. Fig. 8(a)–(d) exhibit the

This article has been accepted for inclusion in a future issue of this journal. Content is final as presented, with the exception of pagination.

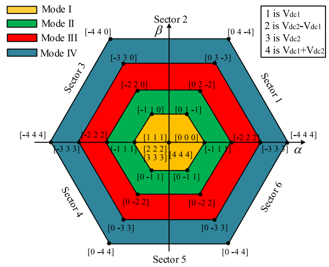

Fig. 9. Space vector representation in $\alpha\beta$-frame with an MPC.

TABLE VI
EFFICIENCY COMPARISON OF PROPOSAL WITH OTHER MSIS

Efficiency	VSI	[9]	[10]	[11]	[12]	Proposed
Mode I	98.2%	93.12%	94.39%	93.38%	95.02%	**96%**
Mode II	98.63%	95.88%	96.39%	95.2%	96.42%	**97.61%**
Mode III	98.9%	98.07%	98.24%	98.10%	98.23%	**98.46%**
Mode IV	98.85%	97.54%	97.82%	97.87%	98.06%	**98.15%**

power losses and efficiency evaluations of the proposed MSI and other conventional MSIs for operation modes I–IV, respectively. Fig. 8 displays that the suggested MSI decreases power losses and has a higher efficiency compared with other MSIs except for VSI. This is due to the fact that in the proposed MSI, the number of ON-state switches that are in the current pass is lower than in other conventional MSI topologies. Table VI gives the efficiency comparison of the proposal with VSI and other reported MSIs. As can be seen, the proposed topology has higher efficiency than [9], [10], [11], and even [12] due to the low number of conductive devices in the current path. The higher efficiency is for standard VSI due to not using extra switches on the dc-link side. It should be noted that to evaluate the operation modes of VSI, similar to other MSIs, we changed the reference current signal. In the first operation modes, the lowest efficiency is for [9] and [11], and the highest efficiency is for VSI and proposal. By changing the operation modes, the effectiveness of the proposal is going to be higher due to using just the same number of devices in the conductive current path for all operation modes. In the first operation mode, VSI and proposal have higher efficiency than other MSIs, which confirms the proposal idea.

By consideration of the compared investigations, we could consider the following benefits of the proposed MSI over other MLIs as a conclusion.

1) Two of the reported MSIs in the literature [9], [10] can generate only three operation modes with the same magnitude of used dc-link voltages with the proposed topology. It means they can produce operation modes V_{dc1}, V_{dc2}, and $V_{\mathrm{dc2}} - V_{\mathrm{dc1}}$, and the two sources cannot be connected in series to achieve a higher overall dc-link voltage. However, the proposed MSI and [11] and [12] can generate one more mode, which is using the overall dc-link voltage $V_{\mathrm{dc1}} - V_{\mathrm{dc2}}$. This allows the dc-bus voltage to be larger than any one source. This can reduce the switching losses even further and will allow the tractive system to maintain peak torque for even higher motor speeds.
2) The presented MSIs [9]–[11] cannot be extended for n dc sources. The proposed MSI and [12] have this capability, which is a suitable configuration for EV energy storage systems.
3) The proposed MSI has a low number of IGBTs and drivers in comparison to [11] and [12], which generate the same number of operation modes.
4) The proposed MSI has a lower number of conductive active components in the current path for each mode compared with [11] and [12]. Therefore, the low conductivity of the devices leads to low conduction losses, which increase efficiency.
5) The TBV of the proposal is lower than similar MSI topologies with the same operation modes. The low voltage stress means low manufacturing costs, which is an important factor for the industry for massive production.

C. Benefits of MSIs Over Single-Source Inverters for EVs

An MSI that utilizes different cells of a battery pack as sources can potentially increase battery lifetime compared with a single-source inverter. Battery cells in a pack can exhibit slight variations in capacity, internal resistance, and health. When using a single-source inverter, all cells are subjected to the same load and discharge cycles, which can lead to imbalance issues over time. In contrast, an MSI can distribute the load more evenly across various cells, reducing the strain on individual cells and improving the overall pack balance.

MSIs with two or more dc sources can provide redundancy in power sources. This means that if one battery pack or energy source fails, the vehicle can still operate using the other sources. This redundancy enhances vehicle reliability and safety. Furthermore, by combining multiple energy sources, such as batteries and supercapacitors, MSIs can deliver bursts of power when needed, potentially resulting in improved acceleration and overall vehicle performance. In addition, an MSI has the capability to manage fast charging from various power supplies, including standard charging stations, high-power dc chargers, and renewable energy sources.

D. DC-Link Capacitor Calculation

The amount of charge and discharge of dc-link capacitor of a traction inverter is obtained

$$\triangle Q_C = \int_0^T I_o \sin(\omega t) d(t) \tag{33}$$

$$\triangle V_C = \frac{\triangle Q_C}{C} = \frac{I_o}{f_s C}(d(1-d)). \tag{34}$$

Therefore, the minimum amount of the capacitance (C_{opt}) according to allowable voltage ripple ($\triangle V_{\mathrm{ripple}(pp)}$) are obtained as

$$C_{\mathrm{opt}} \geq \frac{I_o(d(1-d))}{\bar{f}_s \triangle V_{\mathrm{ripple}(pp)}}. \tag{35}$$

Since the control method of the proposed MSI is MPC, therefore here $\bar{f}_s$ is the average switching frequency of the inverter, I_o is

TABLE VII
PROPOSED MSI AND PMSM PARAMETERS

	Parameters	Values	Units
Proposed Inverter	DC source voltages	$V_{\text{dc1}} = 50$ $V_{\text{dc2}} = 150$	[V] [V]
PMSM	Speed Rating	8000	[r/min]
	Current Rating	28.38	[A]
	Torque Rating	23.9	[N.m]
	Stator resistance (R_s)	0.396	[Ω]
	Inductance ($L_d = L_q$)	2.4	[mH]
	Rotational inertia (J)	1.916×10^{-3}	[kg.m^2]
	Magnetic flux (ψ_m)	0.129	[Kg.m^2]
	B_m	4.64e-3	[N.m.$\frac{\text{rad}}{\text{s}}$]
	Poles pairs number (p)	5	
Times	Sample time (T_s)	40	[μs]
	Subsampled time (T_{sw})	400	[μs]

the steady-state output current, C_{opt} is the optimum required capacitance, $V_{\text{ripple}(pp)}$ is the maximum allowed peak–peak ripple voltage of dc-link, and d is the duty cycle.

VI. SIMULATION RESULTS OF THE PROPOSED MSI

In this section, the proposed MSI is tested by the simulation through the proposed model predictive control in MATLAB/Simulink environment. The parameters of the considered system (input and output) are listed in Table VII.

The MSI operates as a three-phase inverter and drives the PMSM as a motor. In motor drive applications, when both speed and torque references are applied in the same direction, the power is positive, namely, the PMSM generates power and the MSI operates as an inverter. If both speed and torque references have opposite signs, the PMSM generates power and the MSI operates as a rectifier. Hence, the same simulation model presented in Fig. 7 can be used to simulate both operations. The simulation results for both operations are shown in Fig. 10. Simulations in inverter operations are performed at four different speed references (ω), 150, 300, 550, and 750 [rad/s]. The d component of stator reference current $i_d^* = 0$, and a constant load torque T_{load} of 20 N.m is applied to the motor. The speed control of the machine shows good reference tracking, with a fast dynamic response and without observable overshoots or undershoots in both operational modes, as shown in Fig. 10(a). The line-to-line voltage produced by the proposed MSI is shown in Fig. 10(b) illustrating that the MSI works properly and produces the three operation modes based on the demand of the speed that PMSM needs. The a-phase stator current of the PMSM is shown in Fig. 10(c) illustrating that the phase currents are highly sinusoidal, despite the variable switching frequency. The dc current of the two used dc sources of MSI i_{dc1} and i_{dc2} is shown in Fig. 10(d). This figure confirms that when MSI works in mode I, i_{dc1} is a positive value, and i_{dc2} is zero, which means that the second dc source supplies the motor and V_{dc1} not used. Also, it indicates that when MSI works in mode II, the two input dc sources are in series, and the negative pole of the second dc source is connected to the negative pole of the first dc source voltage. Hence, i_{dc2} has a positive value, and i_{dc1} has a negative value. Once MSI works in mode III, the second dc source supplies the motor, and V_{dc1} is not used, so the i_{dc2} is positive and the i_{dc1} is zero. Besides, it indicates that once the proposed MSI works in mode IV, the two input dc sources are in series, and the positive pole of the first dc source is connected to the negative pole of the second dc source voltage. Hence, the i_{dc1} and i_{dc2} have positive values. The stator currents i_d and i_q are shown in Fig. 10(e). The reference current i_q^* is produced by the PI controller and it is tracked by the inner control loop of MPC. The reference current of i_d^* is considered zero and the i_d is followed by the MPC in zero value. As can be seen from Fig. 10(e), the MPC tracks both quadrant stator currents quickly and without any changes in either operational mode. Figs. 11 and 12 show a zoomed view of Fig. 10 in different modes that MSI operates. The steady state of the first operation mode of MSI is shown in Fig. 11(a) between 0 and 0.4[s]. As shown in this figure, the magnitude of V_{AB} is 50[V] and only the first dc voltage source supplies the motor. The steady state of the second operation mode of MSI is shown in Fig. 11(b) between 0.4 and 0.6[s]. This figure confirms that the difference between both dc sources supply the motor so the magnitude of V_{AB} is 100 V. The steady state of the third operation mode of MSI is shown in Fig. 12(a) from 0.6 to 0.8[s]. This figure confirms that the only second dc voltage source supplies the motor so the magnitude of V_{AB} is 150 V. The steady state of the fourth operation modes of MSI for both inverter and rectifier operational modes is shown in Fig. 12(b) between 0.95 and 1.2[s]. This figure confirms that only two used dc voltage sources supply the motor for both operational modes so the magnitude of V_{AB} is 200 V.

Figs. 10–12 confirm that the applied MPC makes a difference between voltage waveforms from mode I and other modes. This difference happens when MSI is controlled by MPC because, as we showed in Fig. 9, to generate modes II–IV, it does not evaluate the zero vector for generating these operation modes. Because MPC operates based on choosing the optimal vector, which is closest vector. The advantage of MPC for the proposed MSI in EV systems is that the harmonic distortion is reduced, which avoids damaging the winding of EMs. In order to validate the theoretical concept of the voltage stress of the switches (12) and (13), all the voltage stress of the switches for the fourth operation mode is shown in Fig. 12(c). As can be seen, none of the switches endure the overall dc-link voltage, which is 200 V. Most of the power switches endure the magnitude of the first dc source (50 V), and the voltage stress of switch S_3 is equal to the second dc source (150 V). Therefore, this figure confirms that the measured values are correct with the theoretical values, to have a comparison of the proposed topology and [12] when both MSIs use in EV applications. In fact, we repeated and performed a similar simulation for [12]. We compared three terms of efficiency, THD, and blocking voltage for each operating mode for the proposed MSI and presented MSI in [12]. The results are given in Table VIII. As can be seen, the efficiency of the proposal is higher than in [12] in operation modes I, III, and IV due to the use of low-active switches (2) for generating these modes. The THD value of the proposal is almost the same as [12]. With increasing the switching frequency as well, you can see the results are higher efficiency and lower THD, but still, the proposal has higher efficiency and lower THD than [12]. The voltage stress on the power switches for the VSI part is the same, but for the MS part, the voltage stress of the switches is lower than [12]. These three advantages can be obtained when the proposal is used for EV rather than other presented MSI in [12].

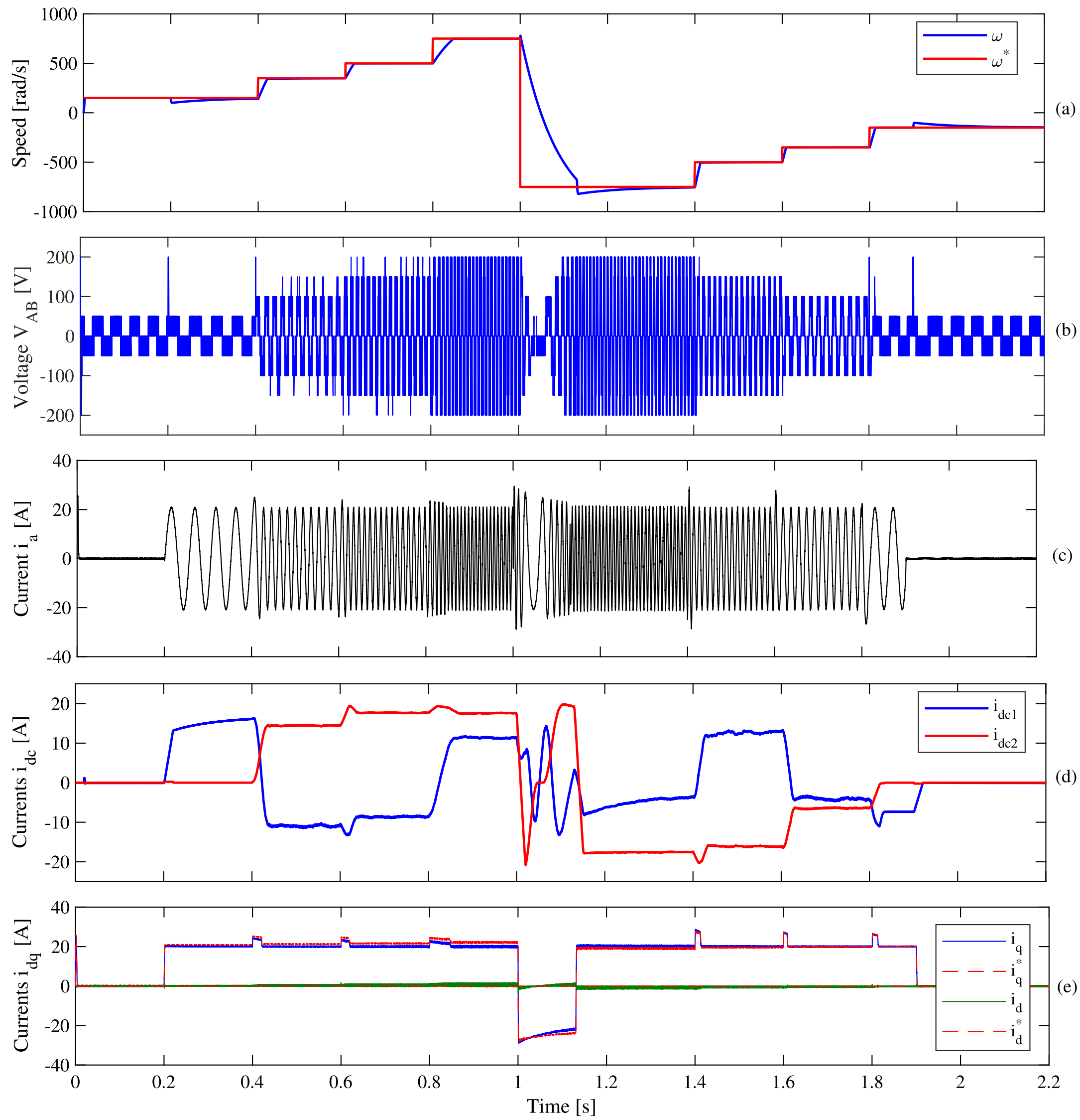

Fig. 10. Dynamic response. (a) Motor speed. (b) Line-to-line voltage. (c) A-phase stator current. (d) DC source currents. (e) Quadrant stator currents.

TABLE VIII
EFFICIENCY, THD, AND TBV COMPARISON OF THE PROPOSED MSI WITH [12]

Topolog	Mode	Efficiency T=40[μs]	THD T=40[μs]	Efficiency T=50[μs]	THD T=50[μs]	TBV [V]
[12]	I	90.35%	1.85%	90.45%	1.62%	650
	II	94.16%	1.08%	94.46%	0.98%	1050
	III	94.67%	1.02%	94.93%	0.82%	1250
	IV	95.58%	1.14%	96.22%	1.01%	1700
Proposed	I	90.30%	1.65%	90.56%	1.43%	550
	II	94.23%	0.96%	94.67%	0.92%	950
	III	95.31%	0.85%	95.59%	0.76%	1200
	IV	96.86%	1.04%	97.13%	0.94%	1550

Table IX illustrates the average switching frequency of each switch in the proposed inverter for sample time 40[μs], T_L=20[N $\cdot$ m], and window time 20[s]. Since the proposed MSI has different operation modes, first the average switching frequency of each switch is calculated for each mode ($\bar{f}_{s,\text{switch}}$=number of commutation/2 window time) separately, and then its value is divided by the total number of operation modes. The frequency of each switch in the proposed topology is different due to the nature of MPC, which has a variable frequency. Note that in this table, the average switching frequency of two switches in each leg of the VSI in the proposed MSI is equal; therefore, only one of them is written.

TABLE IX
AVERAGE SWITCHING FREQUENCY OF SWITCHES FOR T=40[μS]

Switches	S_1	S_2	S_3	S_4	S_5	U_1	U_2	U_3
f_s [Hz]	7675	7675	8885	7483	6067	2465	2460	2440

VII. EXPERIMENTAL RESULTS OF THE PROPOSED MSI

To show the performance of the proposal, the prototype of the proposed MSI is built on a laboratory scale with IGBT power switches. The picture of experimental setup is shown

This article has been accepted for inclusion in a future issue of this journal. Content is final as presented, with the exception of pagination.

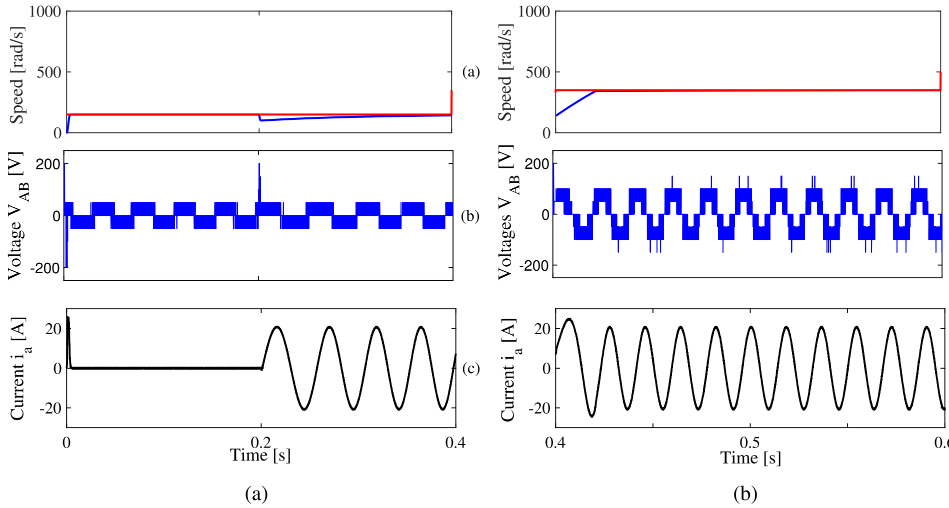

Fig. 11. Simulation results of motor speed, line-to-line voltage, and a-phase current of proposed MSI. (a) First operation mode. (b) Second operation mode.

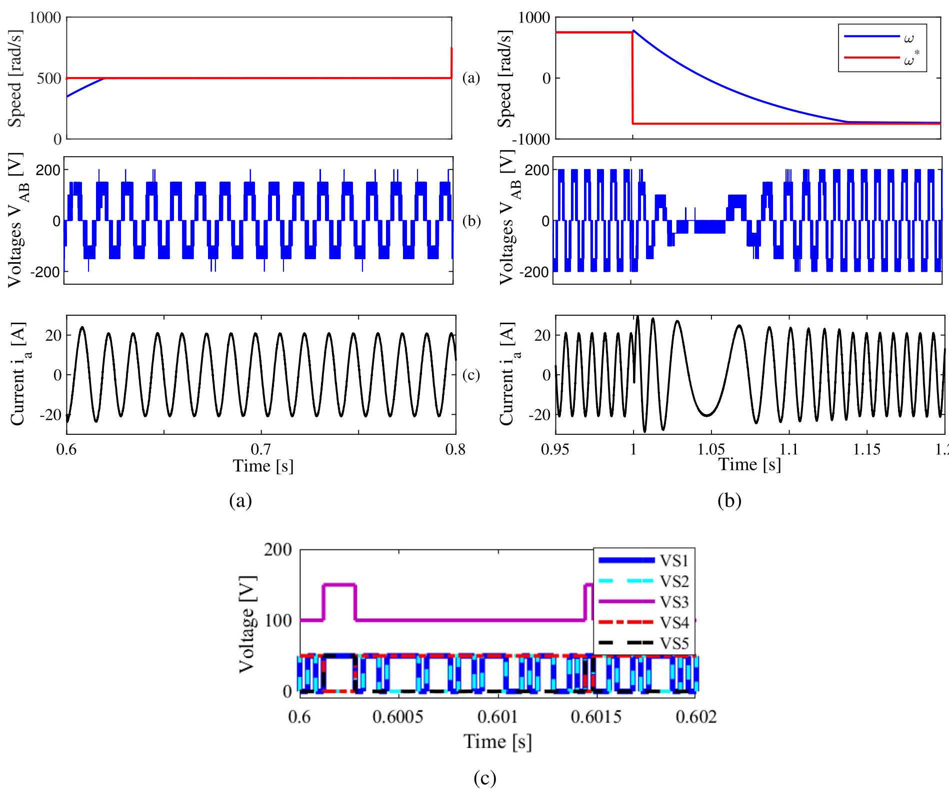

Fig. 12. Simulation results of motor speed, line-to-line voltage, and a-phase current of proposed MSI. (a) Third operation mode. (b) Fourth operation mode. (c) Voltage stress on the power switches of the MS unit.

in Fig. 13. Digital signal processing (DSP) is used to implement the proposed model predictive control. The output of the proposed topology is connected to a static load. The method used for practical evaluations is given in Table X. To show the performance evaluation of each mode of the proposed MSI, model predictive current control is applied. Therefore, with varying the current reference amplitude, all operation modes can be generated. To validate the experimental validation of the first operation mode, the reference current is adjusted to 1[A]. Fig. 14 shows the experimental results for mode I. In this figure, the line–line voltage (V_{ab}) of the MSI, and three-phase load currents (I_{abc}) are shown in Fig. 14(a). In this mode, only the first dc power supply (30[V]) transfer the power to the load. Therefore, the current of the second dc source is zero under this mode as shown in Fig. 14(b). The THD value of current is 1.85%.

This article has been accepted for inclusion in a future issue of this journal. Content is final as presented, with the exception of pagination.

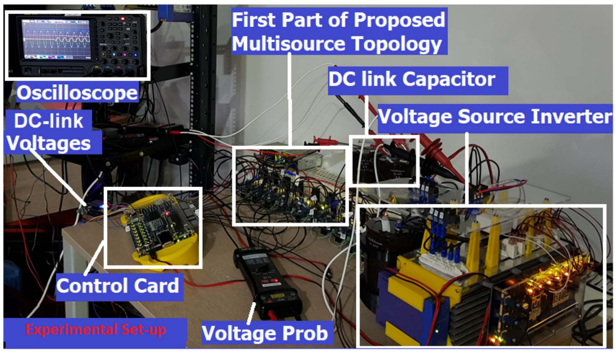

Fig. 13. Experimental setup of the proposed MSI.

TABLE X
EXPERIMENTAL PARAMETERS

Parameters	Values	Units
DC voltages (CHUX-S-1000-0-220)	$V_{dc1} = 30$	[V]
	$V_{dc2} = 90$	[V]
DC-link capacitor	C_1=2.2	[mF]
	C_2=4.7	[mF]
IGBT	IHW20N120R3FKSA1	1200 [V], 40 [A]
Gate driver	HCPL-316J-000E	-
DSP	TMS320F28335	-
Load frequency (f_o)	50	[Hz]
Static load	R, L	10 [Ω], 10 [mH]
Sample time (T_s)	40	[μs]

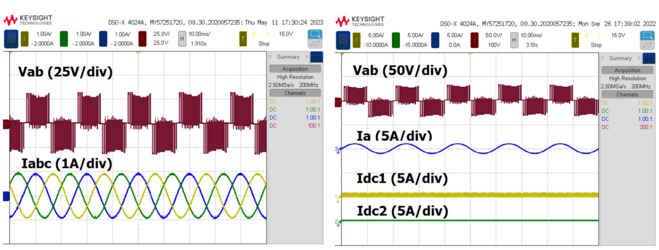

(a) (b)

Fig. 14. Experimental results for the first operation mode. (a) Line-to-line voltage (V_{ab}) and three-phase load current (I_{abc}). (b) Line-to-line voltage, phase current (I_a), and dc source currents ($I_{\mathrm{dc1}}, I_{\mathrm{dc2}}$).

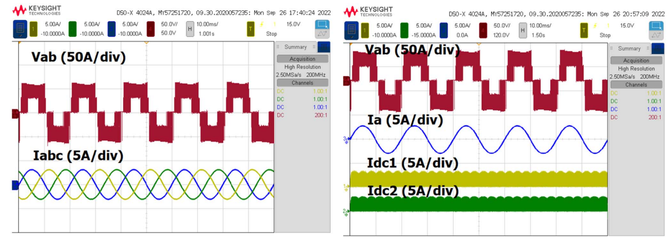

(a) (b)

Fig. 15. Experimental results for the second operation mode. (a) Line-to-line voltage (V_{ab}) and three-phase load current (I_{abc}). (b) Line-to-line voltage, phase current (I_a), and dc currents ($I_{\mathrm{dc1}}, I_{\mathrm{dc2}}$).

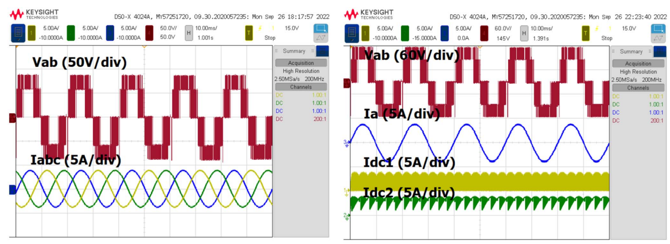

(a) (b)

Fig. 16. Experimental results for the third operation mode. (a) Line-to-line voltage (V_{ab}) and three-phase load current (I_{abc}). (b) Line-to-line voltage, phase current (I_a), and dc currents ($I_{\mathrm{dc1}}, I_{\mathrm{dc2}}$).

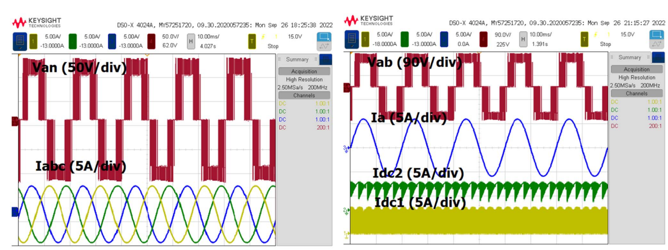

(a) (b)

Fig. 17. Experimental results for the fourth operation mode. (a) Line-to-line voltage (V_{ab}) and three-phase load current (I_{abc}). (b) Line-to-line voltage, phase current (I_a), and dc currents ($I_{\mathrm{dc2}}, I_{\mathrm{dc1}}$).

By increasing the reference current to 3[A], the second operation mode of the proposed MSI is created. The results are shown in Fig. 15. As can be seen, the practical line voltage (60[V]) and load currents are shown in Fig. 15(a) This mode is generated by the subtraction of both dc power supplies. Therefore, they have transferred the power to the load, so the value of dc current in the first dc supply is positive and in the second dc, supply is negative, as shown in Fig. 15(b). The THD value of current for the second mode is 1.16%. The third operation mode of the experiment is achieved by setting the reference load currents to 4[A]. The experimental output waveform is shown in Fig. 16(a). The second dc power supply has transferred the power to the load so the output voltage magnitude is 90[V], as shown in Fig. 16(b). The THD value of current for the third operating mode is 1.05%. The current load reference is increased to 6[A] to show the fourth experiment operation mode of the proposed MSI. In this mode, both dc power supplies are provided the maximum power to the load, so the output voltage is 120[V] under this mode, as shown in Fig. 17(a) and (b). The THD value of current for this mode is 1.24%. From the voltage waveforms displayed in the simulation and experiment, it is clear that model predictive control performs exceptionally well when the operating mode of the proposed MSI shifts. For instance, once the MSI works in the second operation mode, the MPC uses optimal voltage vectors between the first mode and the second mode and does not return to evaluating the zero vector. The output voltage figures confirm the theoretical space vector representation of MPC for the proposed MSI in Fig. 9, in which each operation mode is indicated by different colors. This feature causes dv/dt to reduce, as well as THD and power losses, which are very suitable for EV applications. Fig. 18 depicts the proposed MSI's response when the reference currents shift from 3 to 4[A]. The operation mode of the MSI switches from mode II to mode III by increasing the amplitude of the reference current signals, increasing the

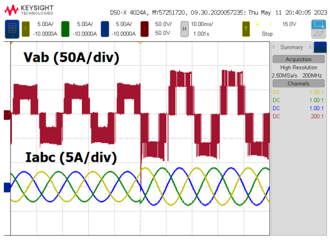

Fig. 18. Experimental results for the evaluation of dynamic response of the proposed MSI: line-to-line voltage (V_{ab}) and three-phase load current (I_{abc}).

peak voltage from 60 to 90[V]. The suggested MPC has a high dynamic response to this variation, as seen in Fig. 18, a low transient time is needed when the current signals are changed. It also demonstrates that the three-phase currents closely follow the reference current signals with a rapid transition time and no current waveform spike.

VIII. Conclusion

This article presented a generalized MSI topology as a traction inverter for EV applications. The proposed inverter was a combination of a multisource unit with a low number of components and a high operation mode, and a standard two-level inverter. The multisource unit provided a variable dc-link voltage, so with a combination of n number of dc sources, it could create a high number of operation modes without using any passive components. The presented traction inverter, in comparison to other MSI topologies, had two benefits: it utilized fewer switches and produced four combinations between the two used dc sources, which considerably decreased the battery pack compared with other MSI topologies. Furthermore, the proposed inverter decreased the power losses and increased the efficiency in comparing other traditional MSIs. A model of predictive control was used to operate the powered traction inverter. The simulation findings demonstrated that the MPC was a promising alternative control approach for EVs due to its simplicity, ability to generate a good waveform, and high performance. A prototype of the proposed inverter was built to verify the correctness of its operation, and it was tested with model predictive control for static loads.

References

[1] Y. Yang, L. Dorn-Gomba, R. Rodriguez, C. Mak, and A. Emadi, "Automotive power module packaging: Current status and future trends," *IEEE Access*, vol. 8, pp. 160 126–160 144, 2020.

[2] L. Dorn-Gomba, J. Ramoul, J. Reimers, and A. Emadi, "Power electronic converters in electric aircraft: Current status, challenges, and emerging technologies," *IEEE Trans. Transport. Electrific.*, vol. 6, no. 4, pp. 1648–1664, Dec. 2020.

[3] A. Chub, D. Vinnikov, F. Blaabjerg, and F. Z. Peng, "A review of galvanically isolated impedance-source DC-DC converters," *IEEE Tran. Power Electron.*, vol. 31, no. 4, pp. 2808–2828, Apr. 2016.

[4] I. Laird, X. Yuan, J. Scoltock, and A. J. Forsyth, "A design optimization tool for maximizing the power density of 3-Phase DC-AC converters using silicon carbide (SiC) devices," *IEEE Trans. Power Electron.*, vol. 33, no. 4, pp. 2913–2932, Apr. 2018.

[5] H. F. Ahmed, H. Cha, and A. A. Khan, "A single-phase buck matrix converter with high-frequency transformer isolation and reduced switch count," *IEEE Trans. Ind. Electron.*, vol. 64, no. 9, pp. 6979–6988, Sep. 2017.

[6] A. Poorfakhraei, M. Narimani, and A. Emadi, "A review of modulation and control techniques for multilevel inverters in traction applications," *IEEE Access*, vol. 9, pp. 24 187–24 204, 2021.

[7] "Traction systems for locomotives and highspeed applications," [Online]. Available: https://library.e.abb.com/public/

[8] "Retrofit traction solutions," [Online]. Available: https://library.e.abb.com/public/

[9] L. Dorn-Gomba, P. Magne, B. Danen, and A. Emadi, "On the concept of the multi-source inverter for hybrid electric vehicle powertrains," *IEEE Trans. Power Electron.*, vol. 33, no. 9, pp. 7376–7386, Sep. 2018.

[10] L. Dorn-Gomba, J. Guo, and A. Emadi, "Multi-source inverter for power-split hybrid electric powertrains," *IEEE Trans. Veh. Technol.*, vol. 68, no. 7, pp. 6481–6494, Jul. 2019.

[11] E. Chemali and A. Emadi, "On the concept of a novel reconfigurable multisource inverter," in *Proc. IEEE Transp. Electrific. Conf. Expo.*, 2017, pp. 707–713.

[12] O. Salari, K. H. Zaad, A. Bakhshai, and P. Jain, "Reconfigurable hybrid energy storage system for an electric vehicle DC-AC inverter," *IEEE Trans. Power Electron.*, vol. 35, no. 12, pp. 12 846–12 860, Dec. 2020.

[13] M. A. Hosseinzadeh, M. Sarebanzadeh, C. F. Garcia, E. Babaei, J. Rodriguez, and R. Kennel, "Reduced multisource switched-capacitor multilevel inverter topologies," *IEEE Trans. Power Electron.*, vol. 37, no. 12, pp. 14 647–14 666, Dec. 2022.

[14] C. F. Garcia, C. A. Silva, J. R. Rodriguez, P. Zanchetta, and S. A. Odhano, "Modulated model-predictive control with optimized overmodulation," *IEEE Trans. Emerg. Sel. Topics Power Electron.*, vol. 7, no. 1, pp. 404–413, Mar. 2019.

[15] M. A. Hosseinzadeh et al., "A new multisource inverter topology for electrical vehicle applications controlled by model predictive," in *Proc. IEEE 48th Annu. Conf. Ind. Electron. Soc.*, 2022, pp. 1–6.

[16] J. Rodriguez et al., "Latest advances of model predictive control in electrical drives-Part I: Basic concepts and advanced strategies," *IEEE Trans. Power Electron.*, vol. 37, no. 4, pp. 3927–3942, Apr. 2022.

[17] J. Rodriguez et al., "Latest advances of model predictive control in electrical drives: Part II: Applications and benchmarking with classical control methods," *IEEE Trans. Power Electron.*, vol. 37, no. 5, pp. 5047–5061, May 2022.

[18] Z. Gao and Q. Lu, "A hybrid cascaded multilevel converter based on three-level cells for battery energy management applied in electric vehicles," *IEEE Trans. Power Electron.*, vol. 34, no. 8, pp. 7326–7349, Aug. 2019.

[19] F. H. Khan, L. M. Tolbert, and W. E. Webb, "Hybrid electric vehicle power management solutions based on isolated andnon-isolated configurations of multilevel modular capacitor-clamped converter," *IEEE Trans. Ind. Electron.*, vol. 56, no. 8, pp. 3079–3095, Aug. 2009.

[20] L. Komsiyska et al., "Critical review of intelligent battery systems: Challenges, implementation, and potential for electric vehicles," *Energies*, vol. 14, no. 18, 2021, Art. no. 5989.

Mohammad Ali Hosseinzadeh (Member, IEEE) was born in Gonbad Kavus, Iran. He received the B.Sc. and M.Sc. degrees (Hons.) in electrical engineering-power from the Islamic Azad University Science & Research Branch, Tabriz, Iran, in 2009 and 2012, respectively, and the Ph.D. degree (Hons.) in electrical engineering-power electronics from the University of Talca, Talca, Chile, in 2023.

He is currently a Postdoctoral Researcher with the Technical University of Munich, Munich, Germany. He is the author or coauthor of more than 40 published technical articles. He also holds two patents in the area of power electronics converters. His research interests include design, modeling, and control of multilevel power converters for electric vehicles and inductive wireless power transfer charging, as well as model predictive control for e-mobility applications.

Dr. Hossienzadeh was a frequent Reviewer of IEEE Transaction on Industrial Electronics and IEEE Transaction on Power Electronics.

Maryam Sarebanzadeh (Member, IEEE) was born in Ahvaz, Iran. She received the B.Sc. and M.Sc. in electrical engineering-electronics and electrical engineering-power degrees from the Islamic Azad University Science & Research Branch, Tabriz, Iran, in 2012 and 2014, respectively, and the Ph.D. degree in the field of power electronics from the University of Talca, Talca, Chile, in 2022.

She is currently a Postdoctoral Researcher with the Technical University of Munich, Munich, Germany. She is the author or coauthor of more than 40 published technical articles and has a patent in the area of power electronics inverters. Her research interests include design, modeling and control of transformerless multilevel inverters in photovoltaic applications.

Cristian F. Garcia (Senior Member, IEEE) received the M.Sc. and Ph.D. degrees in electronics engineering from the Universidad Tecnica Federico Santa Maria, Valparaiso, Chile, in 2013 and 2017, respectively.

From 2017 to 2019, he was with the Engineering Faculty, Universidad Andres Bello, Santiago, Chile, as an Assistant Professor. Since 2019, he has been with the Department of Electrical Engineering, University of Talca, Curico, Chile, where he is currently an Assistant Professor. During 2016, he was a Visiting Ph.D. Student with the Power Electronics Machines and Control Group, University of Nottingham, U.K. His research interests include electric transportation applications, variable-speed drives, and model predictive control of power converters and drives.

Ebrahim Babaei (Senior Member, IEEE) received the Ph.D. degree in electrical engineering from the University of Tabriz, Tabriz, Iran in 2007.

He is the author and coauthor of one book and more than 560 journal and conference papers. He also holds 26 patents in the area of power electronics. His current research interests include the analysis, modeling, design, and control of power electronics converters and their applications, renewable energy sources, and FACTS devices.

Dr. Babaei has been the Editor-in-Chief of the *Journal of Electrical Engineering* of the University of Tabriz, since 2013. He is also currently an Associate Editor for IEEE Transactions on Industrial Electronics, IEEE Transactions on Power Electronics, *Open Journal* of the Industrial Electronics Society, and the *Iranian Journal of Science and Technology*, *Transactions of Electrical Engineering*. He has been the Technical Program Chair, Track Chair, Organizer of different special sessions, and Technical Program Committee Member in the most important international conferences organized in the field of power electronics. Several times, he was the recipient of the Best Researcher Award from the University of Tabriz, and also the 2016 Outstanding Reviewer Award from IEEE Transactions on Power Electronics. Since 2015, he has been on the list of the Top One Percent of the World's Scientists and Academics according to Thomson Reuters' list.

Jose Rodriguez (Life Fellow, IEEE) received the Engineer degree from the Universidad Tecnica Federico Santa Maria, Valparaiso, Chile, in 1977, and the Dr.-Ing. degree from the University of Erlangen, Erlangen, Germany, in 1985, both in Electrical Engineering.

Since 1977, he has been with the Department of Electronics Engineering, Universidad Tecnica Federico Santa Maria, where he was Full Professor and the President. Since 2022, he has been the President of the Universidad San Sebastian, Santiago, Chile, where he has also been a Full Professor, since 2019. He has coauthored two books, several book chapters, and more than 400 journal and conference papers. His main research interests include multilevel inverters, new converter topologies, control of power converters, and adjustable-speed drives.

Dr. Rodriguez was the recipient of a number of Best Paper Awards from various IEEE journals. He is a Member of the Chilean Academy of Engineering. In 2014, he was the recipient of the National Award of Applied Sciences and Technology from the Government of Chile, and in 2015, the Eugene Mittelmann Award from the IEEE Industrial Electronics Society. From 2014 to 2019, he was included in the list of Highly Cited Researchers published by Web of Science.

Ralph Kennel (Senior Member, IEEE) was born in Kaiserslautern, Germany, in 1955. He received the Diploma and Dr.-Ing. (Ph.D.) degrees in electrical engineering from the University of Kaiserslautern, Kaiserslautern, in 1979 and 1984, respectively.

From 1983 to 1999, he worked on several positions with Robert BOSCH GmbH, Germany. Until 1997, he was responsible for the development of servo drives. He was one of the main supporters of VECON and SERCOS interface, two multicompany development projects for a microcontroller and a digital interface especially dedicated to servo drives. Furthermore, he took actively part in the definition and release of new standards with respect to CE marking for servo drives. From 1997 to 1999, he was responsible for "Advanced and Product Development of Fractional Horsepower Motors" in automotive applications. His main activity was preparing the introduction of brushless drive concepts to the automotive market. From 1994 to 1999, he was a Visiting Professor with the University of Newcastle-upon-Tyne, U.K. From 1999 to 2008, he was a Professor of electrical machines and drives with Wuppertal University, Wuppertal, Germany. Since 2008, he has been a Professor of electrical drive systems and power electronics with the Technical University of Munich, Munich, Germany. His research interests include sensorless control of ac drives, predictive control of power electronics, and hardware-in-the-loop systems.